Stator Flux-Regulatory Excitation Control in Converter-Fed Synchronous Machines for Pumped-Storage Variable-Speed Hydropower

Jørgen Hagset Stavnesli and Jonas Kristiansen Nøland, *Senior Member, IEEE*

Pumped-storage hydropower is seen as a promising solution for efficient, large-scale energy storage. One competitive technical solution is the variable-speed hydropower plant (VSHP) configured with a converter-fed synchronous machine (CFSM). These machines are operated with one extra degree of freedom that is not usually optimized, where the CFSM's rotor-side DC excitation interacts with the stator-side AC excitation. Depending on machine loading, the CFSM will be utilized in conditions far from its original design. In order to deal with this issue, this paper presents a stator flux control (SFC) method for regulating VSHPs in a more efficient way by adjusting the field current to prevent the machine from operating with over-magnetization independent of loading condition, as well as better utilizing the stator-fed converter current. Also, the CFSM reduces its rotor current losses and extra stator losses from saturated iron. The derived first-principle analytical equations for the proposed SFC have been validated and analyzed in the Matlab/Simulink environment for a large $45\,\mathrm{MVA}$, $375\,\mathrm{rpm}$ CFSM, with the measured saturation curve as input. Finally, dynamic transitions between different levels of pumping power reveal the SFC's ability to help to maintain a unity stator flux in the machine, enabling optimal operation independent of loading level.

***Index Terms*—Excitation systems (ESs), flux regulation, wound-field synchronous machines (WFSMs), converter-fed synchronous machines (CFSMs), saturation modeling.**

I. INTRODUCTION

THE world is currently facing a transitioning face toward a larger share of renewable technologies [1]–[3]. In this energy transition era, the flexibility of the hydropower plant will be exploited to higher levels than ever before due to the intermittent nature of other renewable resources [3]. One solution to deal with this problem is to incorporate hydropower stations with a converter-fed motor-generator topology, which enables pumped storage variable-speed operation (PSVSO) [4]. This option is viewed as one of the most efficient large-scale energy storage solutions currently known. It can even be utilized by grid-consumers far away from the power plant [5]. Such a system also has grid-supporting capabilities [6], and can help to deal with the future power system's challenges [7].

The machine solutions proposed for variable-speed hydropower plants (VSHPs) are converter-fed synchronous machines (CFSMs) [4], [8] and doubly-fed induction machines (DFIMs) [9]–[14], respectively. The CFSM is usually interfaced with a back-to-back (B2B) full-rated converter, which connects the VSHP to the power grid [15]. The common topologies are the two-level converter (2LC) [16], [17] and the three-level neutral point-clamped converter (3L-NPC) [18]–[20]. However, there are several flexibility and fault-tolerance benefits with the multilevel converter [21], [22]. Fig. 1 depicts the general topology for the CFSM-based VSHP, which is the investigated configuration in this paper.

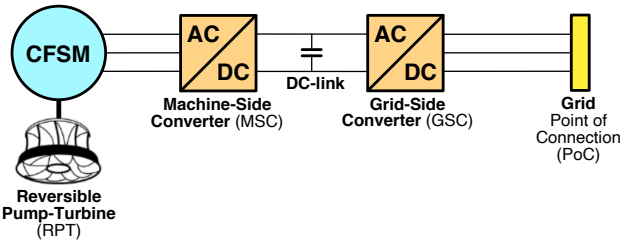

Fig. 1. Illustration of a CFSM configuration for variable-speed hydropower plants (VSHPs) with a reversible pump-turbine. This topology is under investigation herein.

The recent literature has proposed different functionalities for the control system of the VSHP [23], including maximum power point tracking (MPPT) of energy efficiency [24], model predictive control (MPC) [25], active disturbance rejection control (ADRC) [26]. Moreover, due to the inherent complexity of the VSHP, grid-interfacing and governor models have been proposed, where the CFSM has been approximated as a sixth-order [27] and second-order model [28], respectively. Also, improved hydro-turbine controls have been proposed for the PSVSO [29].

This paper deals with the detailed-level modeling of the CFSMs, and their interaction with the excitation system (ES) and the machine-side converter (MSC). The decoupling of the stator and the external grid means that the ES of the CFSM can be used for another purpose other than conventional automatic voltage regulator (AVR) actions. Therefore, in this work, the role of the ES is analyzed with a focus on how the ES can be utilized to improve the operation of the CFSM. Separately excited synchronous machine drives are often controlled to operate with a unity power factor ($\cos\varphi = 1$), where the current and voltage terminal waveforms are in phase. A disadvantage of installing full-sized frequency converters in

Manuscript submitted December 11, 2021; revised April 19, 2022; accepted August 1, 2022 (*Corresponding author: Jonas Kristiansen Nøland*).

This work was supported in part by the Research Council of Norway (RCN) under Grant no. 326673 (SysOpt project).

J. H. Stavnesli is with the Norwegian University of Science and Technology (NTNU), Trondheim, Norway, e-mail: (jorgehst@stud.ntnu.no).

J. K. Nøland is with the Norwegian University of Science and Technology (NTNU), Trondheim, Norway (e-mail: jonas.k.noland@ntnu.no) and also with the University of South-Eastern Norway (USN), Porsgrunn, Norway.

large hydropower plants is the associated converter losses. It is, therefore, of importance to reduce the converter losses by keeping the stator current low, when the converter is not bypassed. One possibility is to reduce this current by taking advantage of the ES's field current regulation (FCR) to achieve the same electrical torque as with rated stator currents. However, a too high field current will saturate the machine, which is an undesirable way of operating the synchronous machine. In order to reduce the stator current while preventing the saturation of the machine, an ES with a stator flux controller (SFC) is proposed in this paper with the objective of maintaining a unitary stator flux magnitude (i.e., $\Psi_s \approx 1.0\,\mathrm{pu}$). This is needed to make the CFSM able to operate with optimal excitation independent of loading level. The primary focus in this paper is put on analyzing the performance of the SFC and comparing it against alternatives which are the power factor control (PFC) of the ES with different FCR levels.

Earlier proposed direct flux control schemes for wound-field synchronous machines (WFSMs) have been proposed to stabilize the torque response under unity power factor control (PFC) [30] and to dynamically decouple the control [31]. There have also been efforts to stabilize the dynamics of the d-axis flux linkage interacting with the field winding [32]. This paper goes beyond recent research by proposing an SFC to supervise the FCR's reference, which can make sure that the stator flux is decoupled from the torque and fully controllable to maximize the magnetic utilization of the machine, independent of loading condition. The main innovation of this work lies in the fundamental treatment of basic WFSM equations to develop a robust stator flux controller that has benefits that can potentially supersede the practice of power factor control in classical variable-speed hydro power applications.

The present paper is organized with the following structure. Section II provides details regarding the handpicked case study and the obtained data from the investigated hydropower plant. Then, a proposed stator flux estimation method is presented in Section III, comparing the performance with and without saturation taken into account. Finally, Section IV presents the main results of the stationary and dynamic performance of the proposed SFC with comparison to conventional approaches, before Section V concludes the paper.

II. Case Description and Obtained Data

A complete schematic diagram of the CFSM topology in Fig. 1 is illustrated in Fig. 3 for pumping mode with its controllers and variables. The DC-link decouples the MSC and the GSC, and therefore, our work focuses on the dynamics of the MSC against the CFSM and the control scheme of the ES by neglecting the GSC. By using the relationship between speed and output power, the machine-side converter indirectly controls the desired power output by regulating the reference speed of the machine. The speed control philosophy relies on aligning the stator current with the q-axis while the d-axis current is regulated to zero ($i_d = 0$) due to the low contribution from the reluctance torque of the given machine's saliency. In this paper, we propose that the ES will regulate the field current to maintain a $1.0\,\mathrm{pu}$ stator flux linkage (Ψ_s). This

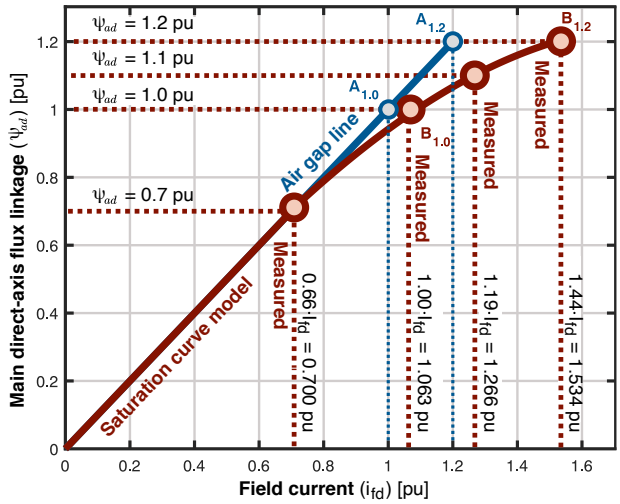

Fig. 2. The per-unit saturation curve of the $45\,\mathrm{MVA}$ synchronous machine aligned with measured operating points at no-load conditions and rated speed $375\,\mathrm{rpm}$.

is achieved with the SFC strategy illustrated in Fig. 4. The controller structure of the alternative SFC has a similar FCR but a different field current reference, based on correcting the power factor (based on estimation) rather than the stator flux.

The studied system was modeled in Matlab/Simulink environment using the Simscape Electrical library. The standard Simulink synchronous machine model is used to model the machine, while an average-value model is used for the converter(s). This simplifies the modeling of the controllers and smooths the shape of the presented results. The controllers for the converters illustrated in Fig.3 was set by Modulus Optimum for the inner control loops and Symmetrical Optimum for the outer control loops. The salient-pole wound-field synchronous machine is rated with $45\,\mathrm{MVA}$, and its key ratings can be found in Table I. Moreover, the machine characteristics were found using classical identification techniques [33], and the standard parameters are reported in Table II. Another important input for modeling is the no-load saturation curve of the machine, which is provided from on-site measurements in Fig. 2. Our saturation curve model is expressed to match the experimentally obtained operating points, which is further explained in Section III. The machine case was handpicked based on similar real-world examples of CFSM systems, e.g., the $100\,\mathrm{MVA}$ Grimsel 2 power plant in Switzerland [34]. It is worth noting that small-scale machines have d-axis time constants more than one order of magnitude smaller than the larger ones. Therefore, the flux regulation becomes a much easier task for smaller compared to larger WFSMs. The paper's objective is to show that the SFC is feasible for large MVA-sized machines and that analytical predictions can verify the legitimacy of the simulations.

III. Stationary Analysis of the CFSM

This section formulates the proposed approach for stator flux estimation of the CFSM based on currents and fluxes at the machine side. The estimation is used to obtain the needed field current reference (i^*_{fd}) for the ES. As flux estimation

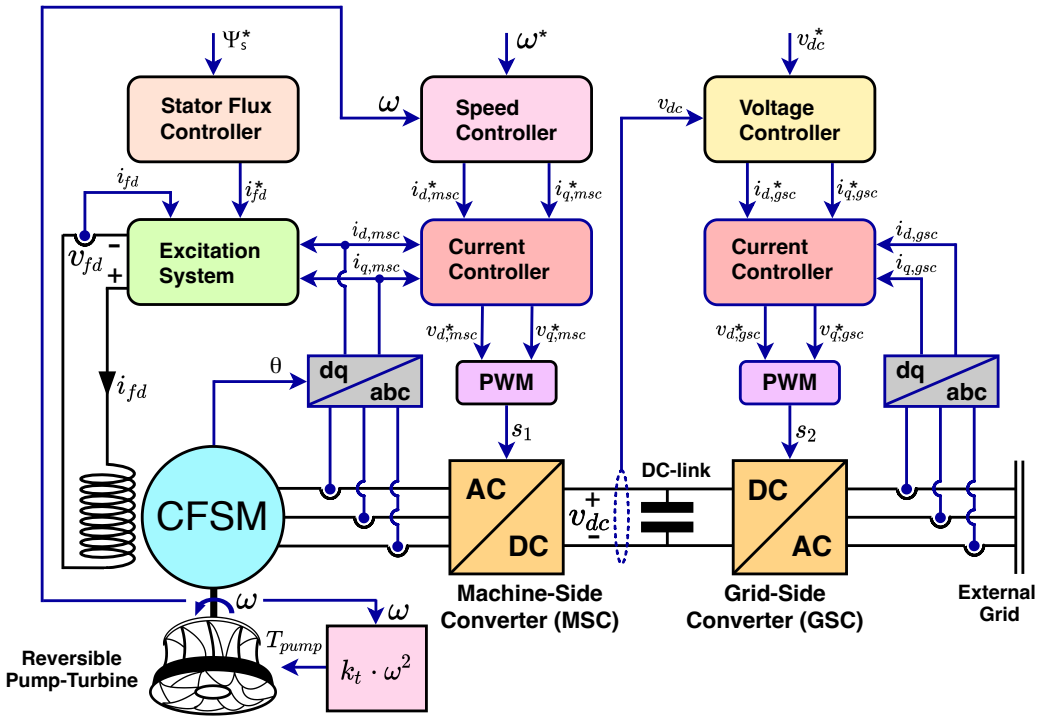

Fig. 3. Overview of the variable speed hydropower CFSM in pump mode and its controllers. The SFC is further described in Fig. 4.

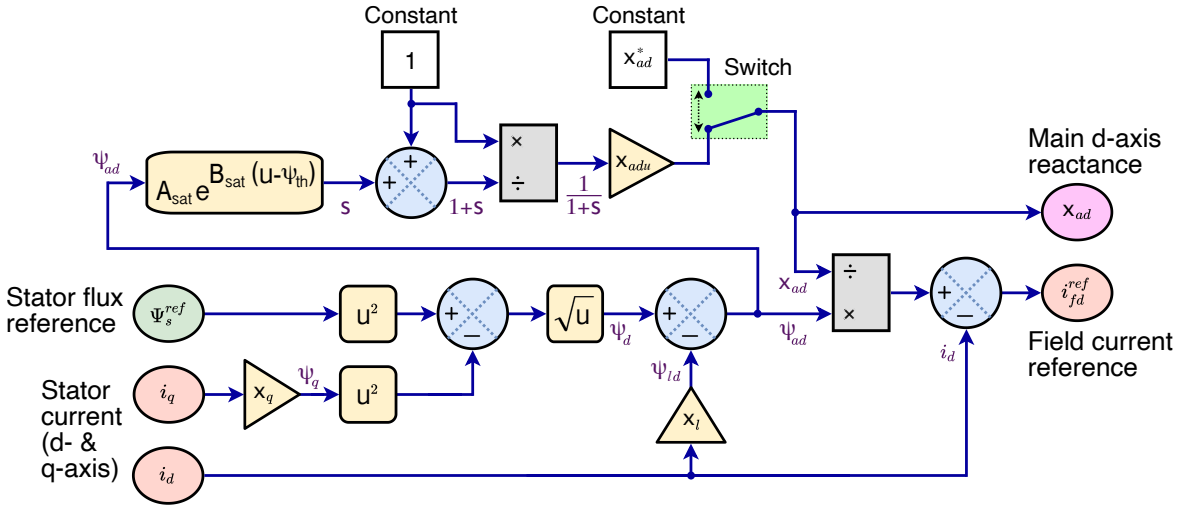

Fig. 4. Overview of the proposed SFC based on eqs. (5) and (12) with i_d and i_q as input variables from the MSC and a saturation model for x_{ad}.

is not readily available in the model environment, a basic stator flux estimation approach was implemented (see Fig. 4), which allowed us to compare the proposed SFC against the alternative PFC. In the dq-equivalent circuit frame, the stator flux (Ψ_s) can be found as a projection of the d- and q- axis flux linkages (ψ_d and ψ_q) in eq. (1) as follows.

$$\Psi_s = \sqrt{\psi_d^2 + \psi_q^2} \tag{1}$$

The equivalent circuit's dq-axis flux linkages, can be expressed further as,

$$\psi_d = x_{ad} i_{fd} + x_d i_d = \underbrace{x_{ad}(i_{fd} + i_d)}_{\psi_{ad}} + x_l i_d, \tag{2}$$

$$\psi_q = x_q i_q = (x_{aq} + x_l) i_q, \tag{3}$$

where x_{ad} and x_d are the main direct axis and the direct axis reactance, i_{fd}, i_d, and i_q are the field current and the direct- and quadrature axis armature current, and ψ_{ad} is the main direct axis flux linkage. In system studies of salient pole synchronous machines, a common assumption is that the q-axis mutual reactance does not saturate, mainly because the q-axis flux is usually quite small in comparison to the d-axis flux (large air gap height in the q-axis). Therefore, x_{aq} is assumed to be constant, independent of the magnetization of the machine such that x_q can be used as a constant parameter in the next equations.

TABLE I
CFSM MACHINE RATINGS IN GENERATOR MODE

Symbol	Description	Value
S	Apparent power	45.0 MVA
P	Active power	42.0 MW
$cos(\varphi)$	Rated power factor	0.933
Q_{max}	Maximum reactive power	16.2 MVAr
Q_{min}	Minimum reactive power	-14.1 MVAr
U	Nominal voltage	10 kV
I	Nominal current	3674 A
f	Nominal frequency	50 Hz
p	Number of poles	16
n	Nominal speed	375 rpm
H	Inertia time constant	2.6 s

TABLE II
OBTAINED STANDARD PARAMETERS OF THE CFSM

Symbol	Description	Value
r_s	stator resistance (20°C/80°C)	0.0024 pu / 0.0030 pu
x_l	leakage react.	0.1700 pu
x_0	zero sequence react.	0.0810 pu
x_2	negative sequence react.	0.1870 pu
x_{adu}, x^*_{ad}	Main d-axis react. (unsat./sat.)	0.7989 pu / 0.7890 pu
x_d	d-axis react. (unsat./sat.)	0.9689 pu / 0.9590 pu
x'_d	d-axis trans. react. (unsat./sat.)	0.3428 pu / 0.2990 pu
x''_d	d-axis sub-trans. react. (unsat./sat.)	0.2279 pu / 0.1980 pu
x_q	q-axis react.	0.6870 pu
x''_q	q-axis sub-trans. react.	0.2430 pu
T'_{d0}	d-axis OC trans. time (sat./unsat.)	5.9170 s / 5.5680 s
T'_d	d-axis SC trans. time (sat./unsat.)	1.3380 s / 1.1630 s
T''_d	d-axis SC sub-trans. time (sat./unsat.)	0.0280 s / 0.0250 s
T''_q	q-axis SC sub-trans. time	0.0380 s

By inserting eqs. (2) and (3) into eq. (1), one obtains

$$\Psi_s = \sqrt{\left(x_{ad} i_{fd} + (x_{ad} + x_l) i_d\right)^2 + \left(x_q i_q\right)^2}. \quad (4)$$

An equation for the optimal field current can then be obtained, yielding

$$i_{fd} = \frac{1}{x_{ad}} \sqrt{\Psi_s^2 - (x_q i_q)^2} - \left(1 + \frac{x_l}{x_{ad}}\right) i_d, \quad (5)$$

which is plotted for variations of i_d and i_q in Fig. 5. These plots visualize how the field current reference of the ES needs to be adjusted to make sure the machine has a unitary stator flux when the loading condition varies, which provides the theoretical basis for the proposed SFC.

A. Stator Flux Controller (SFC)

By setting both Ψ_s =1 pu and $i_d = 0$, eq. (5) can be modified to obtain the field current reference i^*_{fd}, yielding

$$i^*_{fd} = \frac{1}{x_{ad}} \sqrt{1 - (x_q i_q)^2} \quad (6)$$

The field current (i_{fd}) should be regulated according to eq. (5), to keep the stator flux linkage (Ψ_s) constant at 1.0 pu. This strategy is graphically illustrated in Fig. 4, where a saturation model for parameter x_{ad} is incorporated, which will be further described below. The different variables comprising eq. (5) are as follows.

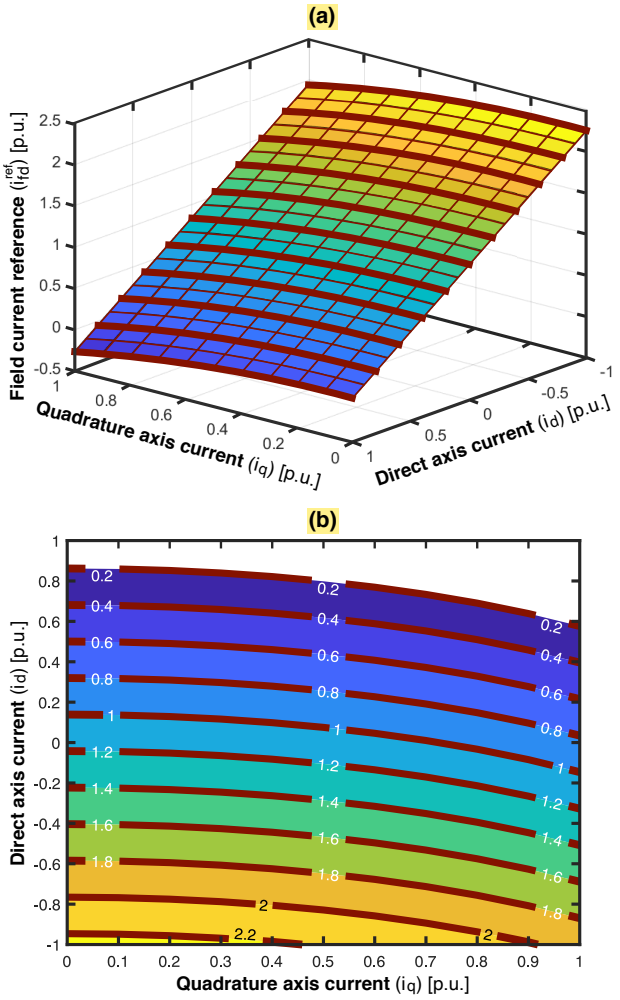

Fig. 5. Plot of the non-saturated field current reference i^*_{fd} from eq. (5) for a 1 pu stator flux (Ψ_s) as a function of d- and q-axis currents (i_d and i_q). The 45 MVA CFSM is considered. **a):** Surface plot. **b):** Contour plot.

1) Two parameters are assumed to be constant, i.e., the quadrature axis reactance (x_q) and the stator leakage reactance (x_l).
2) One parameter, the main direct axis reactance (x_{ad}) is assumed to be a constant up to a certain magnetization level, but depends strongly on the field current (i_{fd}). A saturation curve predicts $x_{ad} = f(\psi_{ad})$, depending on the saturation of the machine.

In order to simplify the strategy, the saturation of the machine can be neglected, which is illustrated in Fig. 4 as a binary switch, assuming a constant main direct axis reactance (x^*_{ad}). However, this approach will only be effective if the machine is operated in a highly under-excited mode, limiting the CFSM's power levels. The dq-axis currents are regulated by the MSC, and the ES sets the stator flux linkage reference to 1.0 pu. The MSC sets the d-axis current reference to zero to maximize the torque generation of the CFSM without reluctance torque. This condition implies that the MSC cannot be operated at unity PFC in the SFC regime. Such control would interact with d-axis current (i_d) that fights against the flux regulation of the proposed ES. As a comparative reference

TABLE III
CONTROL PARAMETERS USED IN THIS PAPER.
INNER CONTROLLERS ARE SET USING MODULUS OPTIMUM, WHILE OUTER CONTROLLERS ARE SET BY SYMMETRICAL OPTIMUM.

Parameter	Power factor controller	Outer-loop speed controller	Field current controller	Quadrature current controller	Direct current controller
Proportional gain (K_p)	$i_{d,ref} = i_q(u_d/u_q)$	$1.584\,\mathrm{pu/pu}$	$1.4854\,\mathrm{pu/pu}$	$1.4064\,\mathrm{pu/pu}$	$1.1459\,\mathrm{pu/pu}$
Integral gain (K_i)	n/a	$71.3\,\mathrm{pu/pu \cdot s}$	$29.4631\,\mathrm{pu/pu \cdot s}$	$5.7199\,\mathrm{pu/pu \cdot s}$	$4.8301\,\mathrm{pu/pu \cdot s}$
Output saturation	n/a	$\omega_{mech} = \pm\ 1.0\,\mathrm{pu}$	$u_{fd} = \pm\ 2.0\,\mathrm{pu}$	$i_q = \pm\ 1.0\,\mathrm{pu}$	$i_d = \pm\ 0.4\,\mathrm{pu}$

to the proposed SFC, a unity PFC can be analyzed with the ES operated as an FCR. All controller parameters considered to study the proposed SFC against the alternative PFC in the case studies presented in Section IV are given in Table III.

B. Saturation Modeling

A further improvement of the SFC is to include saturation of the d-axis main reactance (x_{ad}). This aspect could be neglected, but the effect must be included for achieving an accurate stator flux estimation. The modeling of the d-axis main reactance (x_{ad}) could be made based on a saturation curve depicted in Fig. 2, expressing x_{ad} as a function of the CFSM stator's main direct axis flux linkage (ψ_{ad}). This is done in the region where the true saturation curve diverges from the air-gap line, which occurs for flux levels above $0.7\,\mathrm{pu}$ (ψ_{th}). Based on the data points $A_{1.0}$, $A_{1.2}$, $B_{1.0}$ and $B_{1.2}$ in Fig. 2, two saturation factors (s_{10} and s_{12}) can be found [35], which as given in Table IV. They can be expressed as follows.

$$s_{10} = \frac{B_{1.0} - A_{1.0}}{A_{1.0}} \tag{7}$$

$$s_{12} = \frac{B_{1.2} - A_{1.2}}{A_{1.2}} \tag{8}$$

Then, two saturation constants (A_{sat} and B_{sat}) can be defined as follows [36].

$$A_{sat} = \frac{s_{10}^2}{1.2 \cdot s_{12}} \tag{9}$$

$$B_{sat} = 5 \cdot ln\left(1.2 \cdot \frac{s_{12}^2}{s_{10}}\right) \tag{10}$$

As a result, based on the terminal stator flux linkage of the machines (Ψ_s), a saturation factor (s) can be calculated for all operating points, where

$$s = A_{sat} \cdot e^{B_{sat} \cdot (\psi_{ad} - \psi_{th})} \tag{11}$$

Eq. (11) has a threshold constant, $\psi_{th} = 0.7\,\mathrm{pu}$, which is the point where the saturation curve diverges from the air-gap curve (as seen in Fig. 2).

Finally, x_{ad} can be expressed as

$$x_{ad} = \frac{x_{adu}}{1+s} = \frac{x_{adu}}{1 + A_{sat} \cdot e^{B_{sat} \cdot (\psi_{ad} - \psi_{th})}}, \tag{12}$$

which is incorporated in the proposed SFC illustration in Fig. 4. As already mentioned, this method assumes that x_{ad} is unsaturated (i.e., $x_{ad} = x_{adu}$) until the stator flux linkage reaches $0.7\,\mathrm{pu}$ (ψ_{th}), i.e., $s = 0$. Beyond this, the saturation factor (s) is taken into account when calculating x_{ad}. The stationary characteristic of eq. (12) is plotted in Fig. 6.

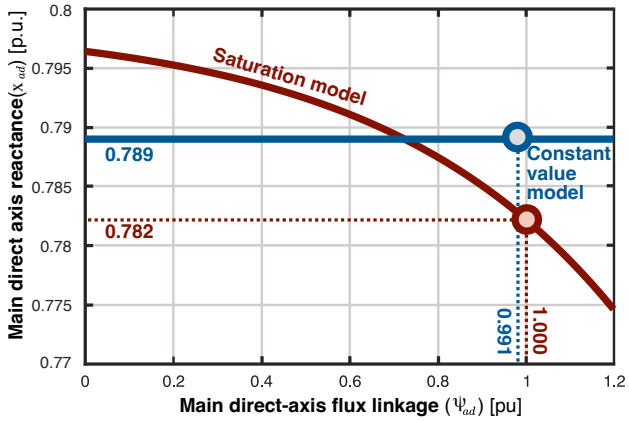

Fig. 6. Main direct axis reactance (x_{ad}) as a function of the stator main direct axis flux (ψ_{ad}), used for SFC. It is based on eq. (12).

C. Electric Load Modeling in Pumping Mode

The pump load is a static model with inertia, where the pumping power is given by a classical cubic relationship with the mechanical speed in SI-units, yielding

$$P_{pump} = k_{pump} \cdot \omega_{mech}^3, \quad T_{pump} = k_{pump} \cdot \omega_{mech}^2, \tag{13}$$

where k_{pump} is defined by the base power (S_b) of the CFSM and the base mechanical speed (ω_b)

$$k_{pump} = \frac{S_b}{\omega_b^3}. \tag{14}$$

In per-unit notation, eq. (13) is reduced such that the per-unit pumping power (P_{pump}) and pumping torque (T_{pump}) is proportional to the per-unit mechanical speed (ω_{mech}) cubed,

$$P_{pump} = \omega_{mech}^3, \quad T_{pump} = \omega_{mech}^2. \tag{15}$$

With $i_d = 0$, the synchronous electrical torque (neglecting reluctance torque and transient damper winding torques) is

$$T_{pump} = \psi_d \cdot i_q, \tag{16}$$

when ψ_d and i_q are amplitude-invariant values in per unit (i.e., factor 3/2 is not necessary).

IV. MAIN RESULTS, VALIDATIONS AND COMPARISONS

This section takes the stator flux estimation method of Section III onboard to analyze further its performances for the case study CFSM described in Section II. First, the proposed SFC is studied with and without taking saturation into account. Then, a benchmark is made with respect to the conventional unity PFC for the converter-fed machine system.

TABLE IV
SATURATION DATA OBTAINED FROM FIG. 2

Parameter	$A_{1.0}$	$A_{1.2}$	$B_{1.0}$	$B_{1.2}$	s_{10}	s_{12}	A_{sat}	B_{sat}	ψ_{th}
Value	1.000 pu	1.200 pu	1.063 pu	1.534 pu	0.063 pu	0.278 pu	0.012 pu	1.933 pu	0.7 pu

TABLE V
ANALYTICAL VALIDATION OF OPERATING POINTS INVESTIGATED IN FIGURE 7, WHERE D-AXIS FLUX IS $\psi_d = x_{ad} i_{fd}$, $i_d = 0$, $\psi_d = \psi_{ad}$, Q-AXIS FLUX IS $\psi_q = x_q i_q$, AND THE TOTAL FLUX LINKAGE IS $\Psi_s = 1$.

i_d	i_q	ψ_d	ψ_q	x_{adu}	i_{fdu}	s	x_{ad}	i_{fd}	i_{fd}^{sim}
0.0 pu	0.0 pu	1.0000 pu	0.0000 pu	0.7989 pu	1.2517 pu	0.0214	0.7821 pu	1.2785 pu	1.278 pu
0.0 pu	0.1 pu	0.9976 pu	0.0687 pu	0.7989 pu	1.2488 pu	0.0213	0.7822 pu	1.2754 pu	1.275 pu
0.0 pu	0.2 pu	0.9905 pu	0.1374 pu	0.7989 pu	1.2398 pu	0.0210	0.7824 pu	1.2659 pu	1.266 pu
0.0 pu	0.3 pu	0.9785 pu	0.2061 pu	0.7989 pu	1.2248 pu	0.0206	0.7828 pu	1.2500 pu	1.250 pu
0.0 pu	0.4 pu	0.9615 pu	0.2748 pu	0.7989 pu	1.2035 pu	0.0199	0.7833 pu	1.2275 pu	1.227 pu
0.0 pu	0.5 pu	0.9392 pu	0.3435 pu	0.7989 pu	1.1756 pu	0.0191	0.7840 pu	1.1980 pu	1.198 pu
0.0 pu	0.6 pu	0.9111 pu	0.4122 pu	0.7989 pu	1.1404 pu	0.0180	0.7847 pu	1.1610 pu	1.161 pu
0.0 pu	0.7 pu	0.8768 pu	0.4809 pu	0.7989 pu	1.0975 pu	0.0169	0.7856 pu	1.1160 pu	1.116 pu
0.0 pu	0.8 pu	0.8354 pu	0.5496 pu	0.7989 pu	1.0457 pu	0.0156	0.7866 pu	1.0620 pu	1.062 pu
0.0 pu	0.9 pu	0.7859 pu	0.6183 pu	0.7989 pu	0.9838 pu	0.0142	0.7877 pu	0.9977 pu	0.9978 pu
0.0 pu	1.0 pu	0.7267 pu	0.6870 pu	0.7989 pu	0.9096 pu	0.0126	0.7889 pu	0.9211 pu	0.9212 pu

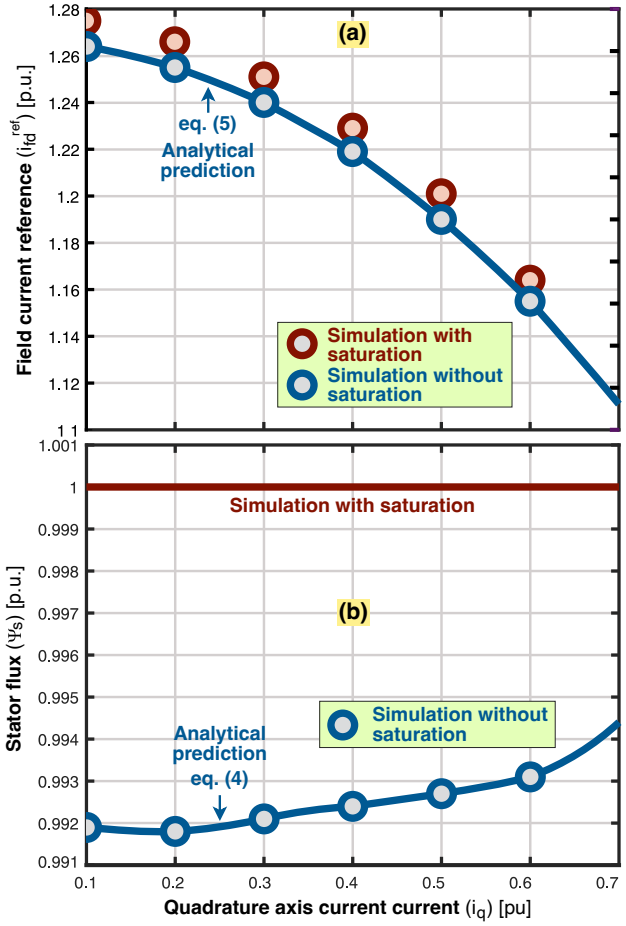

Fig. 7. Validation of the analytical eqs. (4) and (5) against the simulation model for different stationary operating points comparing the field current references producing $\Psi_s = 1\,\text{pu}$ with and without saturation modeling by varying i_q from $0.1\,\text{pu}$ to $0.7\,\text{pu}$, while keeping d-axis current at $0.0\,\text{pu}$. **a)**: Field current reference (i_{fd}^*). **b)**: Stator flux (Ψ_S).

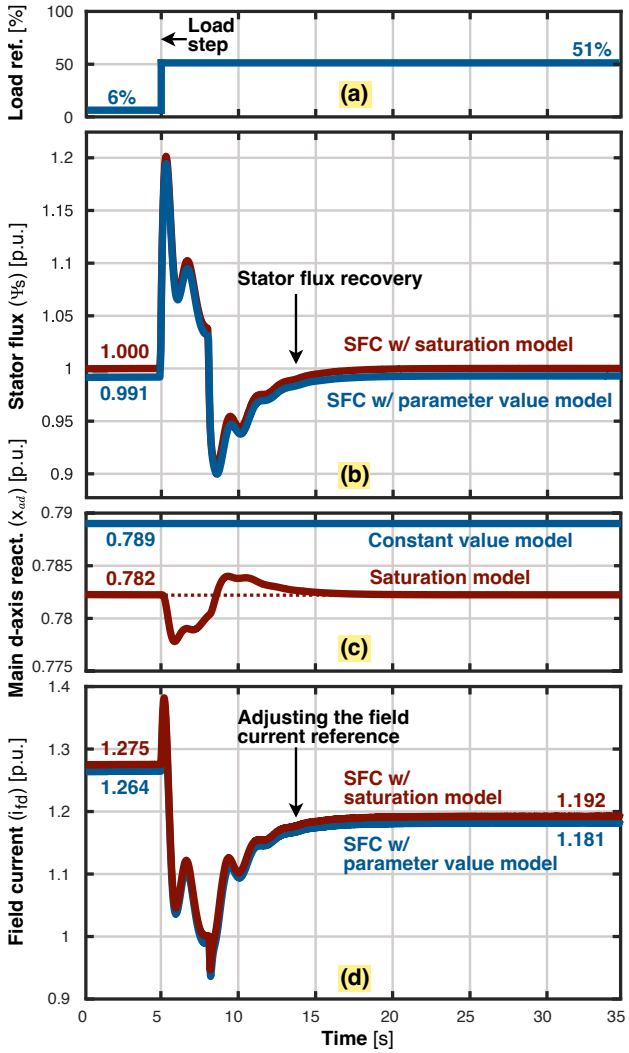

Fig. 8. Comparison between saturation model and constant parameter model. **a)**: Load reference step at time instant $5\,\text{s}$ equivalent to ramping from $6\,\%$ to $51\,\%$ in pumping power, from initial speed $0.4\,\text{pu}$ and then increased to $0.8\,\text{pu}$, used for comparing SFC with and without saturation modelling. **b)**: Stator flux (Ψ_S). **c)**: Main d-axis reactance (x_{ad}). **d)**: Field current (i_{fd}).

A. Analytical Validation of SFC with & without Saturation

In order to examine how the machine is affected by neglecting saturation of the d-axis main reactance (x_{ad}), a stationary validation of the analytical equations are presented in Fig. 7 and Table V, where the predicted i^*_{fd} to achieve unity stator flux agrees well with the simulation model (assessment against simulated i^{sim}_{df} in last column). The transient performance was also investigated by performing a dynamic load step simulation. Here, the machine is simulated in steady-state with $0.06\,\mathrm{pu}$ pumping power and then increased to $0.51\,\mathrm{pu}$, which implies a change in speed from $0.4\,\mathrm{pu}$ to $0.8\,\mathrm{pu}$, following the pump characteristic of eq. (15). The load and the speed are fully coupled in this control scheme. The numerical results are shown in Fig. 8. These plots further indicate the importance of modeling the saturation. By assuming a constant d-axis mutual reactance (x_{ad}), the actual decrease of reactance caused by the increase in machine flux as the speed and voltage reach higher levels is not captured. This leads to a field current reference that is too low, thereby, creating stator magnitude less than $1.0\,\mathrm{pu}$. Moreover, it shows that the inclusion of saturation provides a higher field current reference for the ES to keep the stator flux at $1.0\,\mathrm{pu}$. The difference is, in this case, about $0.9\,\%$. Nevertheless, a noticeable effect is seen, which shows that it will make a difference, especially in highly saturated conditions.

B. Comparison of SFC Against PFC

In this subsection, the SFC is compared to a unity PFC with $\cos(\varphi) = 1$ control for different set points of the field current. These are taken from Fig. 2 as follows.

1) A case where the nominal field current (I_{fd}) is used as the reference for the ES (i.e., i_{fd} =1.063 pu), which is the field current needed to achieve rated machine flux or rate open-circuit terminal voltage ($1.0\,\mathrm{pu}$).
2) An over-magnetized case where the field current is set to $1.19I_{fd}$ (i.e., i_{fd} =1.266 pu), yielding an open-circuit stator flux of $1.1\,\mathrm{pu}$.

The load step simulation considers a case where the reference speed of the machine is changed simultaneously from $0.6\,\mathrm{pu}$ to $1.0\,\mathrm{pu}$. This is equivalent to increasing the pump load from approximately $20\,\%$ to $100\,\%$ loading. The results are shown in Figs. 9, 10, 11, and 12. The load step analysis presents two ways of controlling a variable-speed electrically-excited synchronous machine as follows.

1) Optimal machine operation where the machine is kept out of over-magnetization.
2) Optimal converter operation where the power drawn from the converter is at unity power factor.

These two objectives cannot be achieved simultaneously, as the PFC adjusting the d-axis current (i_d) comes into direct conflict with the SFC on its FCR. This is because both field current and d-axis current will affect the d-axis component of the stator flux vector.

In Fig. 9, the SFC is shown to achieve high transient torque, even though d-axis current can be kept to zero, implying no reluctance torque. This implies that the transition phase of the load step is comparable to the PFC. The main converter benefit of PFC is that the unity power factor is recovered after the load step. However, this is only true if the field current set point is set high enough. As can be seen in Fig. 10a, when the field current is set to 1.00 Ifd, the PFC is not able to fully recover the power factor. This is seen in Fig. 10. However, Fig. 11 shows that only the SFC is able to recover the stator flux after the load step, which is expected as the PFC was, per definition, not intended to achieve this objective. The SFC is even able to mitigate the overshoot in the stator flux by keeping the field current transiently low during the load transition. On the contrary, the PFC gets a high stator flux overshoot but also

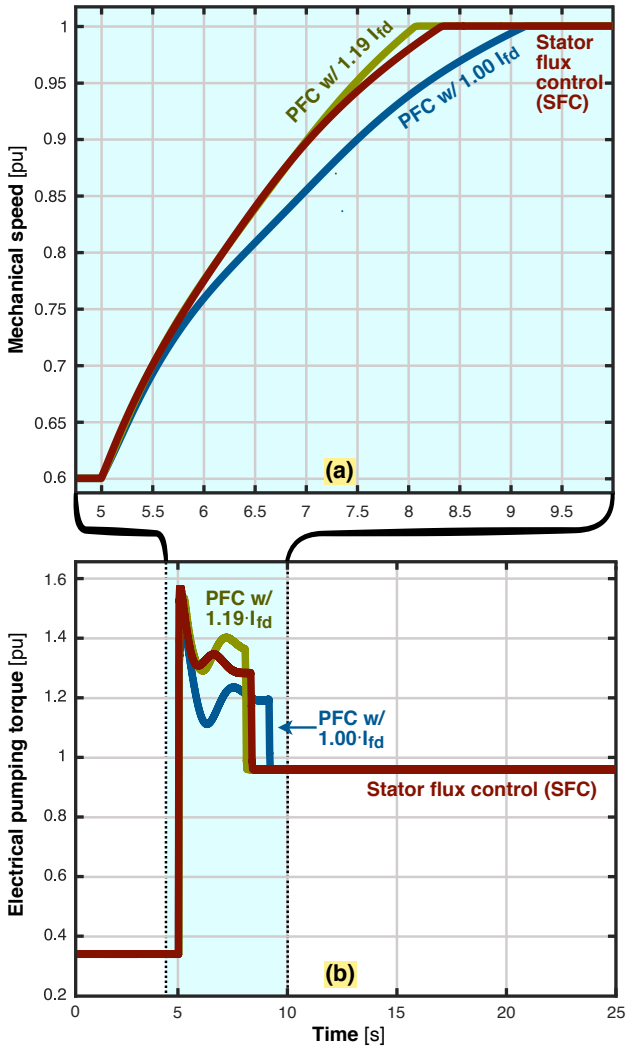

Fig. 9. Speed transition of the CFSM for the different control strategies when ramping pumping power from $20\,\%$ to $100\,\%$. $1.0I_{fd}$ corresponds to i_{fd} =1.063 pu. Similarly, $1.19I_{fd}$ corresponds to i_{fd} =1.266 pu. **a)**: Mechanical speed. **b)**: Electrical pumping torque.

TABLE VI
INITIAL AND FINAL STATOR FLUX (Ψ_s) BEFORE AND AFTER THE SPEED TRANSITION IN FIGS. 8-11, COMPARING THE DIFFERENT METHODS

Method	Initial	Final
Stator flux control (SFC)	1.000 pu	1.000 pu
PFC w/ $1.00 \cdot I_{fd}$	0.904 pu	1.309 pu
PFC w/ $1.19 \cdot I_{fd}$	1.030 pu	1.330 pu

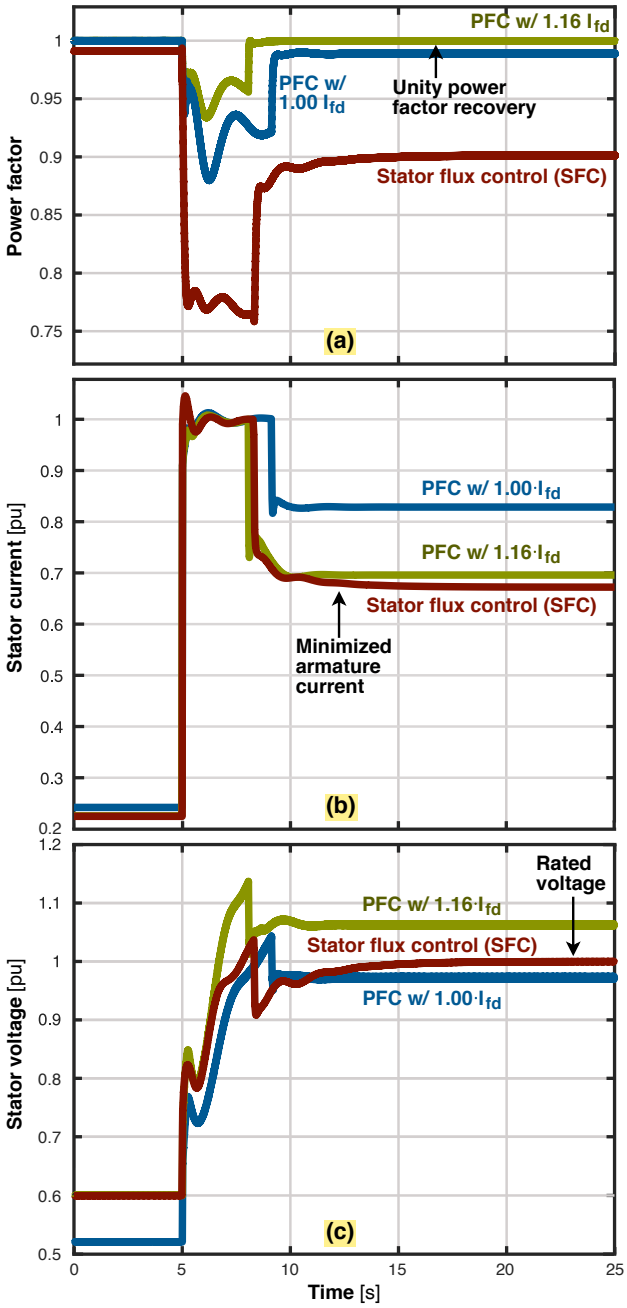

Fig. 10. The load step is the same as presented in Fig. 9. **a)**: Power factor. **b)**: Stator current. **c)**: Stator voltage.

over-magnetization after the transition. This fact emphasizes the ability of the SFC to prevent the machine from becoming over-saturated after ramping up the pump load. The SFC is the only approach that can keep unity stator flux in the CFSM, satisfying the optimal flux regulation, independent of loading. This is further highlighted in Table VI, where a high over-magnetization is indicated for the PFC ($\geq 30\,\%$) after the load step. This is due to the fact that a higher loading level in the stator armature creates an additional flux linkage that the ES does not compensate against under PFC, as i_{fd} is controlled to be constant.

In addition to the above, the SFC indicates better torque-per-ampere performance than the PFC method, as seen in Fig.

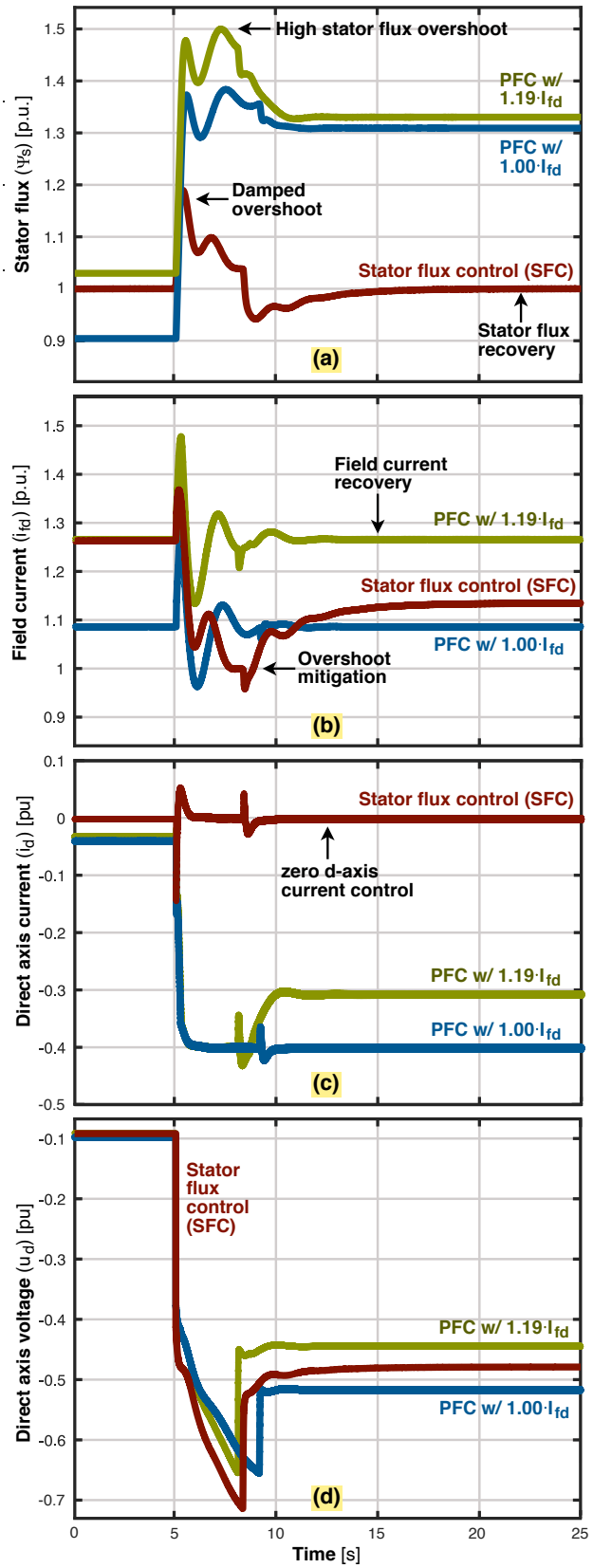

Fig. 11. Assessment of the different control strategies for same case as Fig. 9. **a)**: Stator flux (Ψ_S). **b)**: Field current (i_{df}). **c)**: Direct axis stator current (i_d). **d)**: Direct axis stator voltage (u_d).

12. This is due to the fact that only the torque producing q-axis current of the converter is used, while the d-axis current is regulated to zero. For the PFC, the d-axis current is used to improve the overall power factor of the converter, seen in Figure 10, meaning that the stator (and converter) current will be higher.

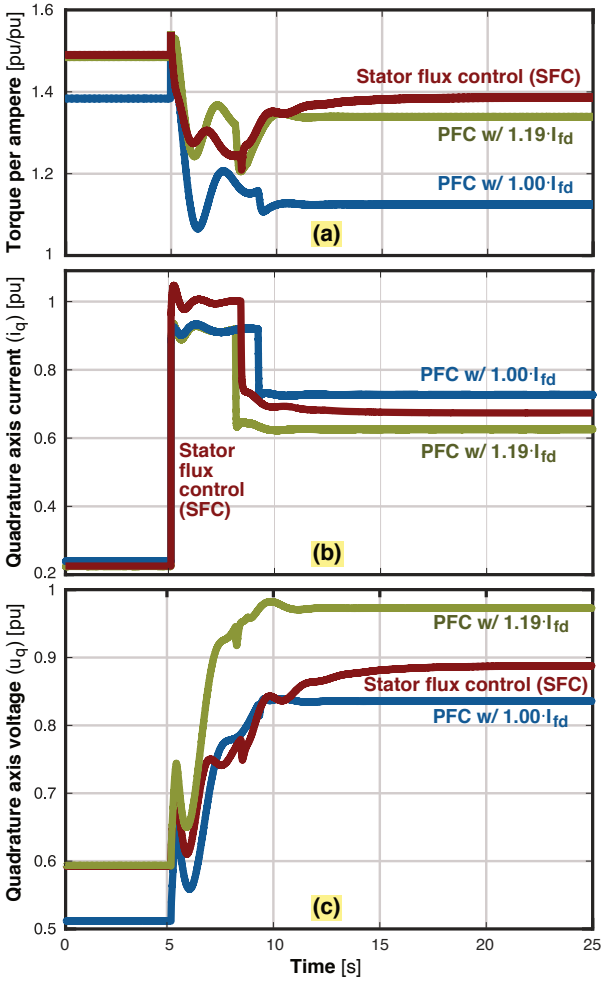

Fig. 12. Assessment of the different control strategies for same case as Fig. 9. **a)**: Torque per ampere. **b)**: Quadrature axis stator current (i_q). **c)**: Quadrature axis stator voltage (u_q).

C. Further Discussion

The benefit of utilizing SFC is that the machine is operated without over-magnetization, which is beneficial for the operation of the electrical machine. While the $\cos(\varphi) = 1$ control method maintains a unity power factor, thus minimizing reactive converter power, the decrease in power factor is rather small for the SFC method while keeping unitary stator flux. On the contrary, the main benefit of the PFC is the optimal converter operation. However, it does not yield any better gains over the SFC method because the current drawn by the machine from the converter was, in fact, found to be higher. The acceleration of the machine is comparable for all control methods and will be less important because the main function of a VSHP is its ability to vary its load optimally. It is worth mentioning that a fast frequency response measure was considered out of the scope of this study.

V. Conclusion

This paper presents a method to optimally control CFSMs by using the field current to maintain a unitary stator flux magnitude (i.e., $1.0\,\mathrm{pu}$). The proposed SFC method achieves a better torque-per-ampere performance than a unitary PFC method at the converter-side. The PFC relied on using the d-axis current component of the converter to operate at unity power factor. While the $\cos(\varphi) = 1$ control method minimizes reactive converter power, it inevitably draws a higher current, potentially nullifying the gains of a higher power factor than the SFC approach. In addition, the machine losses with PFC control will be higher due to the over-magnetized operation of the machine and the higher field current losses in the rotor, thus reducing the overall machine efficiency. Still, the SFC shows comparable acceleration with the PFC control method. One of the limitations of this paper is that it focuses on one particular case study on a detailed level to emphasize the robustness of the proposed SFC. However, more case studies could have been conducted to enlarge the performance evaluated, and dedicated hardware results could be extracted from a large MVA-sized generator with relevant time constants.

Future research items could involve examining and comparing machine losses due to magnetization against power losses in the converter to get a clearer picture of the potential performance improvements in terms of overall energy efficiency for the complete conversion system. This could provide further evidence to support the SFC method as more beneficial than operating the machine with a unity power factor. More work could also be done on the stator flux estimation, taking measurement errors into account and which are less dependent on the inductance values of the machine. Additionally, the tuning of the controller parameters could be further studied, especially the speed of response of the FCR of the ES. Finally, some sort of hybrid control strategy could be examined, particularly for low-speed operations where magnetization losses may be less important than power losses in the converter. In addition to the electrical modeling, further work could also include more details in modeling the mechanical subsystem for variable-speed applications.

References

[1] J. Markard, "The next phase of the energy transition and its implications for research and policy," *Nature Energy*, vol. 3, no. 8, pp. 628–633, 2018.
[2] L. Kitzing, M. K. Kofoed Jensen, T. Telsnig, and E. Lantz, "Multifaceted drivers for onshore wind energy repowering and their implications for energy transition," *Nature Energy*, pp. 1–10, 2020.
[3] W. Yang, P. Norrlund, L. Saarinen, A. Witt, B. Smith, J. Yang, and U. Lundin, "Burden on hydropower units for short-term balancing of renewable power systems," *Nature Communications*, vol. 9, no. 1, pp. 1–12, 2018.
[4] M. Valavi and A. Nysveen, "Variable-speed operation of hydropower plants: A look at the past, present, and future," *IEEE Ind. Appl. Mag.*, vol. 24, no. 5, pp. 18–27, 2018.
[5] T. Tellefsen, J. van Putten, and O. Gjerde, "Norwegian hydropower: Connecting to continental europe," *IEEE Power and Energy Mag.*, vol. 18, no. 5, pp. 27–35, 2020.
[6] T. I. Reigstad and K. Uhlen, "Variable speed hydropower for provision of fast frequency reserves in the nordic grid," *IEEE Trans. Power Syst.*, pp. 1–1, 2021.

[7] Z. Dong, J. Tan, E. Muljadi, R. M. Nelms, A. St-Hilaire, M. Pevarnik, and M. D. Jacobson, "Developing of quaternary pumped storage hydropower for dynamic studies," *IEEE Trans. Sustain. Energy*, vol. 11, no. 4, pp. 2870–2878, 2020.

[8] B. Li, Z. Duan, X. Wang, and J. Wu, "Loss-of-excitation analysis and protection for pumped-storage machines during starting," *IET Renew. Power Gen.*, vol. 10, no. 1, pp. 71–78, 2016.

[9] A. Joseph, K. Desingu, R. R. Semwal, T. R. Chelliah, and D. Khare, "Dynamic performance of pumping mode of 250 MW variable speed hydro-generating unit subjected to power and control circuit faults," *IEEE Trans. Energy Convers.*, vol. 33, no. 1, pp. 430–441, 2018.

[10] A. Joseph, S. Kim, S. Sing Lee, A. Dominic, and K. Lee, "Boost multi-level npc-fed vs large rated asynchronous pumped storage hydro-generating unit," *IET Electr. Power Appl.*, vol. 13, no. 10, pp. 1488–1496, 2019.

[11] A. Joseph, R. Selvaraj, T. R. Chelliah, and S. V. A. Sarma, "Starting and braking of a large variable speed hydrogenerating unit subjected to converter and sensor faults," *IEEE Trans. Ind. Appl.*, vol. 54, no. 4, pp. 3372–3382, 2018.

[12] A. Joseph, T. R. Chelliah, R. Selvaraj, and K. Lee, "Fault diagnosis and fault-tolerant control of megawatt power electronic converter-fed large-rated asynchronous hydrogenerator," *IEEE J. Emerg. Sel. Topics Power Electron.*, vol. 7, no. 4, pp. 2403–2416, 2019.

[13] K. Desingu, R. Selvaraj, and T. R. Chelliah, "Control of reactive power for stabilized junction temperature in power electronic devices serving to a 250-mw asynchronous hydrogenerating unit," *IEEE Trans. Ind. Appl.*, vol. 55, no. 6, pp. 7854–7867, 2019.

[14] Y. Pannatier, B. Kawkabani, C. Nicolet, J. Simond, A. Schwery, and P. Allenbach, "Investigation of control strategies for variable-speed pump-turbine units by using a simplified model of the converters," *IEEE Trans. Ind. Electron.*, vol. 57, no. 9, pp. 3039–3049, 2010.

[15] I. Sami, N. Ullah, S. M. Muyeen, K. Techato, M. S. Chowdhury, and J. S. Ro, "Control methods for standalone and grid connected micro-hydro power plants with synthetic inertia frequency support: A comprehensive review," *IEEE Access*, vol. 8, pp. 176 313–176 329, 2020.

[16] A. Joseph and T. R. Chelliah, "A review of power electronic converters for variable speed pumped storage plants: Configurations, operational challenges, and future scopes," *IEEE J. Emerg. Select. Topics Power Electron.*, vol. 6, no. 1, pp. 103–119, 2018.

[17] J. Koutnik, "Frades ii—variable speed pumped storage project and its benefit to the electrical grid," in *Proc. Int. Conf. Renew. Energy*, 2012, pp. 1–7.

[18] R. R. Semwal, R. Selvaraj, K. Desingu, T. R. Chelliah, and A. Joseph, "Two-stage protection circuit for a multichanneled power electronic converter fed large asynchronous hydrogenerating unit," *IEEE Trans. Ind. Appl.*, vol. 55, no. 6, pp. 5947–5959, 2019.

[19] R. Selvaraj, K. Desingu, T. R. Chelliah, D. Khare, and C. Bharatiraja, "Fault tolerant operation of parallel-connected 3L-neutral-point clamped back-to-back converters serving to large hydro-generating units," *IEEE Trans. Ind. Appl.*, vol. 54, no. 5, pp. 5429–5443, 2018.

[20] K. Desingu, R. Selvaraj, T. R. Chelliah, and D. Khare, "Effective utilization of parallel-connected megawatt three-level back-to-back power converters in variable speed pumped storage units," *IEEE Trans. Ind. Appl.*, vol. 55, no. 6, pp. 6414–6426, 2019.

[21] M. Basić, A. Schwery, and D. Dujić, "Highly flexible indirect modular multilevel converter for high power pumped hydro storage plants," in *Proc. 46th Ann. Conf. IEEE Ind. Electron. Soc.*, 2020, pp. 5290–5295.

[22] A. Joseph, T. R. Chelliah, and K. Lee, "Multi-channel vsi fed large variable speed asynchronous hydro-condenser: fault analysis, fault diagnosis and fault tolerant control," *IET Renew. Power Gen.*, vol. 13, no. 3, pp. 438–450, 2019.

[23] R. Kumari, K. Desingu, T. R. Chelliah, and S. V. A. Sharma, "Development trends and future prospects of hydro-turbine control systems," in *Proc. IEEE Ind. Appl. Soc. Ann. Meet.*, 2019, pp. 1–10.

[24] L. Belhadji, S. Bacha, I. Munteanu, A. Rumeau, and D. Roye, "Adaptive MPPT applied to variable-speed microhydropower plant," *IEEE Trans. Energy Convers.*, vol. 28, no. 1, pp. 34–43, 2013.

[25] L. Ji, Y. Shao, J. Sun, and L. Shi, "Research on self-starting strategy of variable speed pumped storage units based on model predictive control," *J. Eng.*, vol. 2017, no. 13, pp. 984–989, 2017.

[26] L. Ji, J. Sun, M. Zhou, and W. Tian, "AC excitation control strategy of variable speed pumped storage units based on active disturbance rejection control," *J. Eng.*, vol. 2017, no. 13, pp. 1195–1199, 2017.

[27] T. I. Reigstad and K. Uhlen, "Variable speed hydropower conversion and control," *IEEE Trans. Energy Convers.*, vol. 35, no. 1, pp. 386–393, 2020.

[28] L. Wang, Q. Han, D. Chen, C. Wu, and X. Wang, "Non-linear modelling and stability analysis of the ptgs at pump mode," *IET Renew. Power Gen.*, vol. 11, no. 6, pp. 827–836, 2017.

[29] R. Kumari, K. K. Prabhakaran, K. Desingu, T. R. Chelliah, and S. V. A. Sarma, "Improved hydroturbine control and future prospects of variable speed hydropower plant," *IEEE Trans. Ind. Appl.*, vol. 57, no. 1, pp. 941–952, 2021.

[30] Y. Nie, I. P. Brown, and D. C. Ludois, "Deadbeat-direct torque and flux control for wound field synchronous machines," *IEEE Trans. Ind. Electron.*, vol. 65, no. 3, pp. 2069–2079, 2018.

[31] Y. Han, X. Wu, G. He, Y. Hu, and K. Ni, "Nonlinear magnetic field vector control with dynamic-variant parameters for high-power electrically excited synchronous motor," *IEEE Trans. Power Electron.*, vol. 35, no. 10, pp. 11 053–11 063, 2020.

[32] D. Hwang and B.-G. Gu, "Field current control strategy for wound-rotor synchronous motors considering coupled stator flux linkage," *IEEE Access*, vol. 8, pp. 111 811–111 821, 2020.

[33] "Ieee draft guide for synchronous generator modeling practices and parameter verification with applications in power system stability analyses," *IEEE P1110/D06, December 2018*, pp. 1–91, 2019.

[34] A. S. AG, "Case note: 100 mva power converter for variable speed pumped hydropower," 2014.

[35] "Ieee recommended practice for excitation system models for power system stability studies," *IEEE Std 421.5-2016 (Revision of IEEE Std 421.5-2005)*, pp. 1–207, 2016.

[36] V. Vittal, J. D. McCalley, P. M. Anderson, and A. Fouad, *Power system control and stability*. John Wiley & Sons, 2019.

Jørgen Hagset Stavnesli received the MSc. degree in electrical power engineering from Norwegian Univerisity of science and technology in 2020. He is currently employed at ABB Marine and Ports, primarily working on system studies related to ABB's Onboard DC-Grid^{TM} for marine vessels. He has previously been co-author of the article *Performance Analysis of Oustaloup Approximation for the Design of Fractional-Order Analogue Circuits* during a stay at the Technical University of Brno (VUT).

Jonas Kristiansen Nøland (Senior Member, IEEE) was born in Drammen, Norway, in 1988. He received the M.Sc. degree in electric power engineering from the Chalmers University of Technology, Gothenburg, Sweden, in 2013, and the Ph.D. degree in engineering physics from Uppsala University, Uppsala, Sweden, in 2017. Since 2018, he has been an Associate Professor with the Department of Electric Power Engineering, Norwegian University of Science and Technology. His current research interests include excitation systems, hydrogenerators, large AC machines, and enhancing their utilization. Dr. Nøland serves as an Associate Editor for the IEEE TRANSACTIONS ON ENERGY CONVERSION and the IEEE TRANSACTIONS ON INDUSTRIAL ELECTRONICS.